DOI: 10.1590/2317-4889201720170027

ARTICLE

The influence of methane fluxes on the sulfate/methane interface in sediments from the Rio Grande Cone Gas Hydrate Province, southern Brazil

A influência dos fluxos de metano na interface sulfato/metano em sedimentos de hidrato de gás do Cone do Rio Grande, Sul do Brasil

Luiz Frederico Rodrigues[1]*, João Marcelo Ketzer[1], Rogerio Véscia Lourega[1], Adolpho Herbert Augustin[1], Gesiane Sbrissa[1], Dennis Miller[2], Roberto Heemann[1], Adriano Viana[2], Antonio Fernando Menezes Freire[2], Sadoon Morad[3]

ABSTRACT: Much research has been published regarding the relation between major gas hydrate accumulations and the global carbon cycle. In this context, the determination of the sulfate/methane interface (SMI) depth is of primary importance in order to understand the dynamics of methane flux in the shallow section. This paper identifies the depth of the SMI in sediments based on sulfate and methane concentration profiles in cores recovered in the Rio Grande Cone Gas Hydrate Province, Pelotas Basin, southern Brazil. The shape of methane and sulfate concentration profiles in the sediments can be linked to the local methane flux rate as follows: (i) near linear, high upward-diffusing methane flux coupled with high sulfate diffusion from seawater; (ii) irregular, variable methane flux rates; and (iii) kink-type profile, which is indicative of variable rather than strictly high upward methane flux. The areas in which a high methane flux was identified are spatially associated with gas chimneys in sediments within pockmarks, whereas profiles with low methane flux are present in adjacent areas. These chimneys appear as acoustic blankings in seismic records and can therefore be mapped in subsurface. The wavy-like seismic reflection following the SMI coincides with the occurrence of authigenic carbonate nodules and concretions. In addition, high methane fluxes and the occurrence of concretions and nodules carbonates were correlated by stratigraphic position of the concretions bearing intervals and sulfate profiles.

KEYWORDS: gas hydrate; methane flux; Rio Grande Cone; Brazil.

RESUMO: *Muitas pesquisas têm sido publicadas relacionando elevadas acumulações de hidrato de gás e o ciclo global do carbono. Nesse contexto, a determinação da profundidade da interface sulfato/metano (SMI) é importante para entender a dinâmica do fluxo de metano em locais rasos. Este artigo científico identifica a profundidade da SMI em sedimentos com base em perfis de concentração de sulfato e metano em testemunhos recuperados na Província do Hidrato de Gás do Cone do Rio Grande, Bacia de Pelotas, no Sul do Brasil. A forma dos perfis de concentração de metano e sulfato nos sedimentos pode ser relacionada à taxa de fluxo de metano da seguinte forma: (i) fluxo de metano quase linear, de alta difusão ascendente, com alta difusão de sulfato da água do mar; (ii) fluxo de metano irregular e taxas variáveis;(iii) perfil de tipo torção, que é indicativo de um fluxo de metano variável em vez de somente alto fluxo ascendente. As áreas em que o alto fluxo de metano foi identificado estão associadas com chaminés de gás em sedimentos dentro de pockmarks, enquanto perfis com baixo fluxo de metano estão presentes em áreas adjacentes. Essas chaminés aparecem como brancos acústicos nos dados sísmicos e, portanto, podem ser mapeadas na subsuperfície. A variação da reflexão sísmica que segue o SMI coincide com a ocorrência de nódulos e concreções de carbonato autigênicos. Além disso, elevados fluxos de metano e a ocorrência de concreções e nódulos de carbonatos foram correlacionados pela posição estratigráfica dos intervalos de concreções e perfis de sulfato.*

PALAVRAS-CHAVE: *hidrato de gás; fluxo de metano; Cone de Rio Grande; Brasil.*

[1]Pontifícia Universidade Católica do Rio Grande do Sul – PUCRS, Porto Alegre (RS), Brasil. *E-mails: frederico.rodrigues@pucrs.br, jketzer@pucrs.br, rogerio.lourega@pucrs.br, adolpho.augustin@pucrs.br, gesbrissa@gmail.com, roberto.heemann@pucrs.br*

[2]PETROBRAS/CENPES, Rio de Janeiro (RJ), Brasil. *E-mails: miller@petrobras.com.br, aviana@petrobras.com.br, afmfreire62@gmail.com*

[3]The Petroleum Institute, United Arab Emirates University, Sas Al Nakhl (Abu Dhabi), United Arab Emirates. *E-mail: smorad@pi.ac.ae*

*Corresponding author.

Manuscript ID: 20170027. **Received in:** 03/02/2017. **Approved in:** 06/22/2017.

INTRODUCTION

Methane in gas hydrates is generated by bacterial degradation of organic matter at shallow depths below seafloor and/or sourced from deep petroleum fields (Demirbas 2010, Gupta 2004). Methane in deep-sea sediments is transported by advection and diffusion in pore water and, under favorable conditions of pressure, temperature and saturation, part of the methane fluxing through sediments forms methane hydrate within the pore space (Gupta 2004, Demirbas 2010).The consumption of methane owing to microbial activity may increase carbonate alkalinity, which can promote the precipitation of authigenic carbonates (Kennicutt *et al.*1988a, 1988b,Michaelis *et al.* 2002, Sassen *et al.*1998, Matsumoto *et al.* 2011).

Anaerobic oxidation of methane (AOM) and the closely linked sulfate reduction (SR) are dominant processes in organic-rich sediments. AOM occurs at or close to the boundary between SR zone and the methanogenic zone, where methane diffuses upward. The boundary between these two zones is called sulfate/methane interface (SMI).Upward fluxes of methane may affect the depth of SMI below the seafloor (Borowski *et al.* 1996).

Pore water geochemical parameters suggest that most of the upward flux of methane is oxidized anaerobically near the SMI. The occurrence of AOM primarily at the SMI is indicated by a linear sulfate profile in areas with large amounts of methane diffusing upwards (Borowski *et al.* 1996, 1997, Niewöhner *et al.* 1998, Hinrichs*et al.* 1999). AOM can be represented by the reaction ahead (Eq. 1):

$$CH_4 + SO_4^{2-} \rightarrow HCO_3^- + HS^- + H_2O \quad (1)$$

In which:
CH_4 = methane
SO_4^{2-}= sulfate
HCO_3^-= hydrogencarbonate
HS^-= bisulfide
H_2O = water

Immediately below the SR zone and the SMI there is the methanogenic zone, in which methane concentrations increase with depth (Claypool &Kaplan 1974).

Another important anaerobic microbial reaction occurs when sulfate is used as an oxidant by consortium of microorganisms to breakdown organic matter. The reduction of sulfate results in a concave-down exponential profile of sulfate (Berner 1980). This reaction is depicted ahead (Eq. 2):

$$2CH_2O + SO_4^{2-} \rightarrow 2HCO_3^- + H_2S \quad (2)$$

In which:
$2CH_2O$ = formaldehyde
SO_4^{2-}= sulfate
HCO_3^- = hydrogencarbonate
H_2S = hydrogen sulfide

According to Equations 1 and 2, the increase in carbonate alkalinity (primarily HCO_3^-) owes to the decomposition of methane or organic matter (Raiswell 1988).

Organic matter and methane are the fuels for microbial activity in sediments, contributing to the control of the biogeochemical zonation below the seafloor. Geochemical zoning includes the reduction of sulfate as one of the main features of metabolic activity in marine sediments. Therefore, the SMI tends to be located at shallow depths below the seafloor (Hensen *et al.* 2003, Joye *et al.* 2004).

Evidence suggests that there is a relationship between sulfate concentration gradients and upward methane flux rate, which is in equilibrium with underlying gas hydrate systems (Joye *et al.* 2004). Hence, understanding sulfate depletion patterns can be useful for indicating the presence of gas hydrate in sediments (Zatsepina & Buffett 1997, Carroll1992, Borowski *et al.* 1999).

The purpose of this paper was to identify the depth of the SMI in sediments based on sulfate and methane concentration profiles in cores obtained from Rio Grande Cone Gas Hydrate Province, Pelotas Basin, southern Brazil. Additionally, the shape and relationships between these profiles are used in order to estimate the upward methane flux in the sediments. In this manner, this study may provide important information for the understanding of the global carbon cycle and for the exploration of gas hydrates.

STUDY AREA AND GEOLOGICAL SETTING

The study area is located in the Rio Grande Cone (Martins *et al.* 1972), which is a large protuberance in the continental slope of the Pelotas Basin, southern Brazil (Fig. 1). The Pelotas Basin has an area of approximately 250,000 km^{2}resulted from the rifting of Gondwana and the drifting of the South American plate, having accumulated a thick sedimentary package (up to 12 km) from the Barremian to the Recent. The main structures present in the basin are normal faults in the proximal extensional domain and folds and thrust faults in the distal compressional domain (Silveira &Machado 2004).Distinct bottom simulating reflectors (BSRs) are ubiquitous in the Rio Grande Cone, and have been used as the main evidence for the occurrence of large gas hydrate deposits in the Pelotas Basin in Brazil (Sad *et al.* 1998, Fontana & Mussumeci 1994, Clennell 2000,Oliveira *et al.* 2010, Miller *et al.* 2015) and in Uruguay (Tomasini *et al.* 2011).

SAMPLES AND METHODS

Sub-bottom profiler

Sub-bottom profiler (SBP) survey lines were acquired in the study area using an EdgeTech DW106 SBP (Chirp 1–6 kHz, central frequency 3.5 kHz) on board a C-Surveyor II Autonomous Underwater Vehicle (AUV). The AUV was towed at 40 m above the seafloor. The collected lines were processed and visualized using the software HIS Kingdom suite.

Piston cores

Five representative sediment cores were extracted with a 6-m-long piston core device during the MR11oceanographic mission. The cores were named PC01, PC51, PC52, PC53 and PC41 and were recovered in water depths from 531 to 1,301 m. PC41 is a background core. Immediately upon piston core recovery on deck, the Polyvinyl chloride (PVC) liner containing the sediments was removed from the external pipe and cut into 100 cm sections. Sediments and liners were then split lengthwise into a working half,

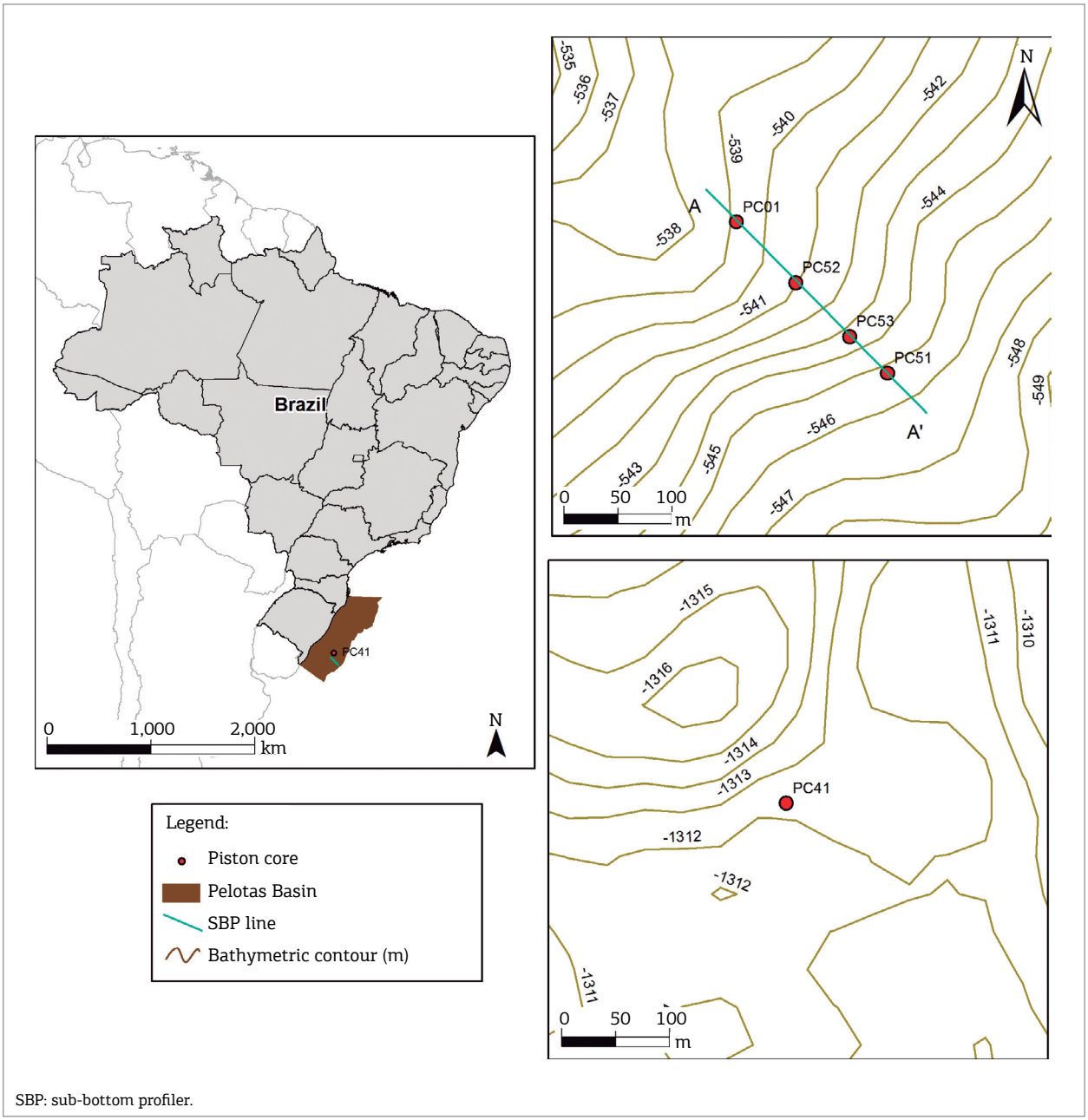

SBP: sub-bottom profiler.

Figure 1. Location map of the Pelotas Basin on the left. Inset on the upper right displays the location of piston cores PC01, PC52, PC53 and PC51 over a sub-bottom profiler line. Inset on the lower right displays the location of piston core PC41. Locations of PC41 and the sub-bottom profiler line are also shown in the location map of the Pelotas Basin.

for sampling, and an archive half, for onboard core descriptions and future storage. Core descriptions involved the annotation of visual grain size, sediment color, icnofacies and structures.

Interstitial water and sediment sampling

The sediment samples of the working half were collected at regular intervals of 30 cm (three per core section) for chemical analysis of the interstitial water. The sediment samples (pieces of 10 to 20 cm) were squeezed onboard using stainless steel hydraulic squeezers, and interstitial water samples were collected in 50 mL syringes attached to the base of each squeezer. Approximately, 10 mL of the interstitial water were used for onboard analysis while 40 mL were transferred to plastic bottles and stored at 4ºC for further analyses onshore.

Sediment samples for gas analyses (C_1-C_5 hydrocarbons) were also collected from the top of the each section in regular intervals of 100 cm. Samples were collected from the freshly exposed tops of the core sections using a spatula and were immediately placed in IsoJars (special plastic container). The sediment samples filled one third of the IsoJars, while another third was filled with distilled water, leaving the top third with air (headspace). Five drops of the diluted Zephiran Chloride bactericide were added into the IsoJars in order to eliminate microbial activity. The IsoJars were kept refrigerated at 4ºC.

Experimental procedures and measurements

Alkalinity was determined using a single beam spectrophotometer (V-1 100D) adjusting the wavelength to 590 nm. Standards with known alkalinity (840, 1,680 and 3,360 mg L^{-1}) were prepared by dilution of a titrated $NaHCO_3$ solution in an aqueous solution. The experimental points demonstrated a first order function with coefficient of determination of 0.997. These equations are used for the calculation of unknown alkalinity samples (Breland & Byrne 1993). The indicator was prepared by mixing in a 250 mL volumetric flask: 5 mL of 98% methanoic acid and 25 mL of a solution of Bromophenol-Blue (500 mg L^{-1}). The final volume was adjusted to 250 mL with a solution of NaCl 0.7 mol L^{-1}. Standards and samples were prepared by mixing 1.5 mL of indicator with 1.5 mL of prepared alkalinity standards or sea water samples in polypropylene tubes and thoroughly shaken to achieve the CO_2 outgassing. Samples above 800 mg L^{-1}were carefully diluted to a known factor by a solution of NaCl 0.7 mol L^{-1} in order to keep the same ionic strength.

Sulfate concentrations in the interstitial waters were determined using a Metrohm (Herisau, Switzerland) ion chromatograph (IC) consisting of a pump (IC liquid handling unit) and a conductivity detector (Model 819). The analytical column was a Metrosep A Supp 5 (150 × 4 mm i.d.) with packing material composed by polyvinyl alcohol with quaternary ammonium groups and particle size of 5 m. A guard column Metrosep A Supp 4/5 Guard, packed with the same material and particle size of analytical column, was also used. An anion self-regeneration suppressor from Metrohm (Model 833 suppressor unit) was used to reduce the conductivity of mobile phase. Samples were diluted using 18 MΩ water, and the standards were also made from pure reagents and 18 MΩ water. Standard solutions were measured repeatedly in order to estimate the accuracy and external precision of the measurement.

A gas chromatograph equipped with a capillary column VP-Plot Alumina/KCl, 30 m × 0.53 mm, Film 10.0 μm, was used to determineC_1-C_5 hydrocarbons concentration in sediments. The GC-14A is configured with a 0.5 mL injection, split 1:7and a flame ionization detector (FID) for gas detection. Run conditions for column were 75ºC; ramping up at 30 to 170ºC, and held for 10 min. Helium was used as the carrier gas at a constant volume of 5 mL/min. The injector temperature was 190ºC and the FID temperature was held at 200ºC.

RESULTS

Sub-bottom profiler

Gas chimneys have been recognized in other regions of the world as displaying typical acoustic blanking features in the SBP records (Riedel *et al*. 2006, Römer *et al*. 2012, Freire *et al*. 2011). In the present study area, detailed high-resolution acoustic surveys using SBP show internal reflections with strong positive amplitudes overlying zones of acoustic blanking which probably represent gas chimneys (Fig. 2A). In contrast, in the background area no amplitude anomalies or blanking features are observed (Fig. 2B). Note that the depth of the SMI, which will be further discussed, is generally shallower in the area with gas chimneys (Fig. 2A) than in the background area (Fig. 2B). Furthermore, it is also observed that the SMI depth is shallower above more intense amplitude anomalies (*e.g.*, PC 51, Fig. 2A).

Piston core descriptions

The four representative piston cores selected for this study (PC52,PC01, PC53, PC51) and the background piston core (PC41) were described as follows (Fig. 3).

PC01(4.38 m long/531 m water depth) consists of homogeneous green gray mud, without grain size

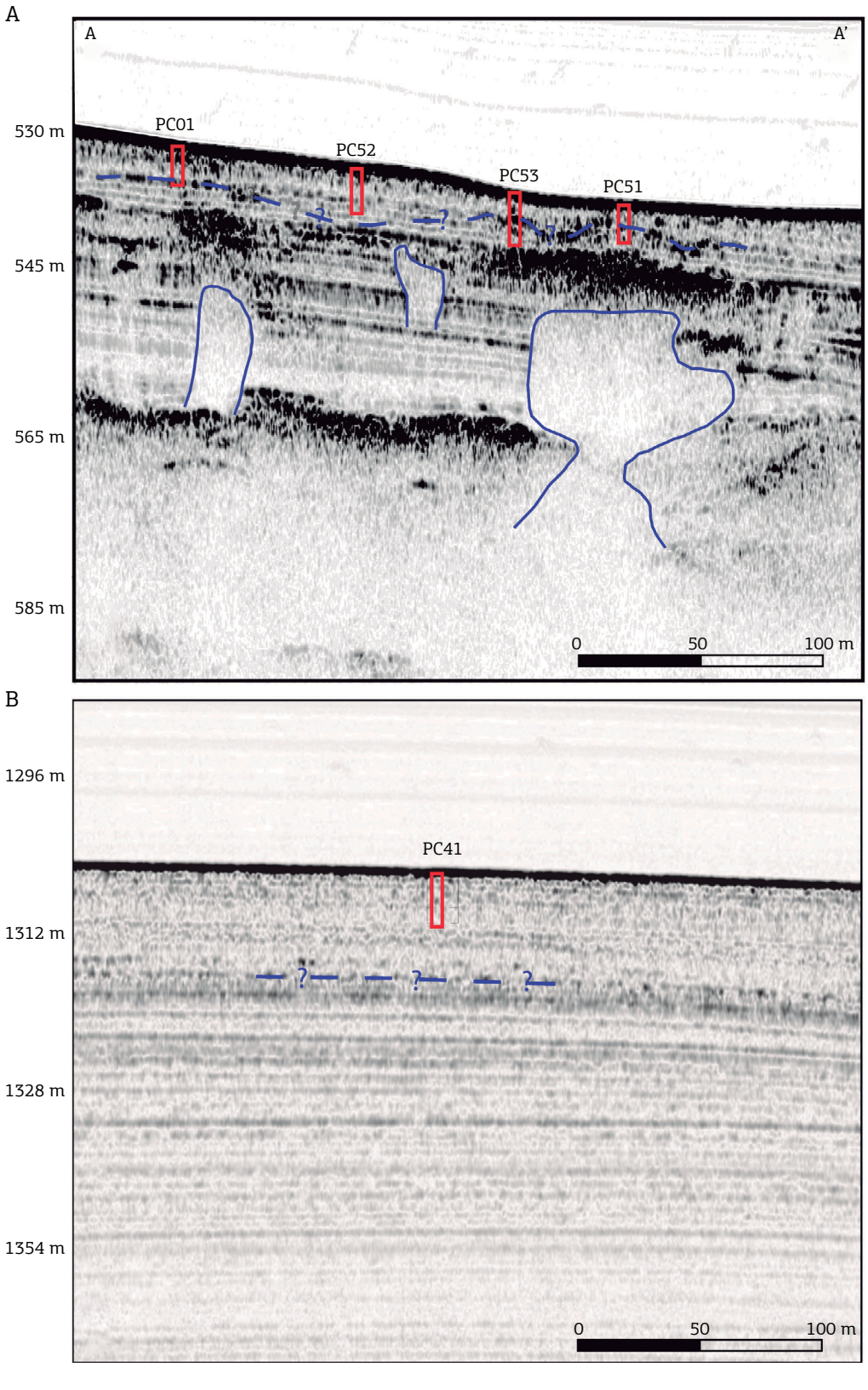

Figure 2. High-resolution sub-bottom profiler images (3.5 kHz) showing: (A) profile in a high-flux gas area with acoustic blanking associated with gas chimneys in the sediment column (solid blue lines); (B) profile in a background area without gas chimneys. The dashed blue lines indicate the inferred position of the sulfate/methane interface, estimated from sulfate and methane concentrations obtained in the cores. The red rectangles are the projected location of the piston cores. The numbers at the left hand side are depth values.

variation, stained by hydro-troilite (a rare iron sulfide mineral with the simple formula of FeS) and showing Thalassinoides ichnofossils (410–438 cm below seafloor (cmbsf)).

PC52 (5.15 m long/532 m water depth) consists of green gray mud with occurrence of hydrotroilite (430 – 445 cmbsf), and *Zoophycos* ichnofossils dispersed below 250 cmbsf. *Burrows* are encountered at 180 to 230 cmbsf.

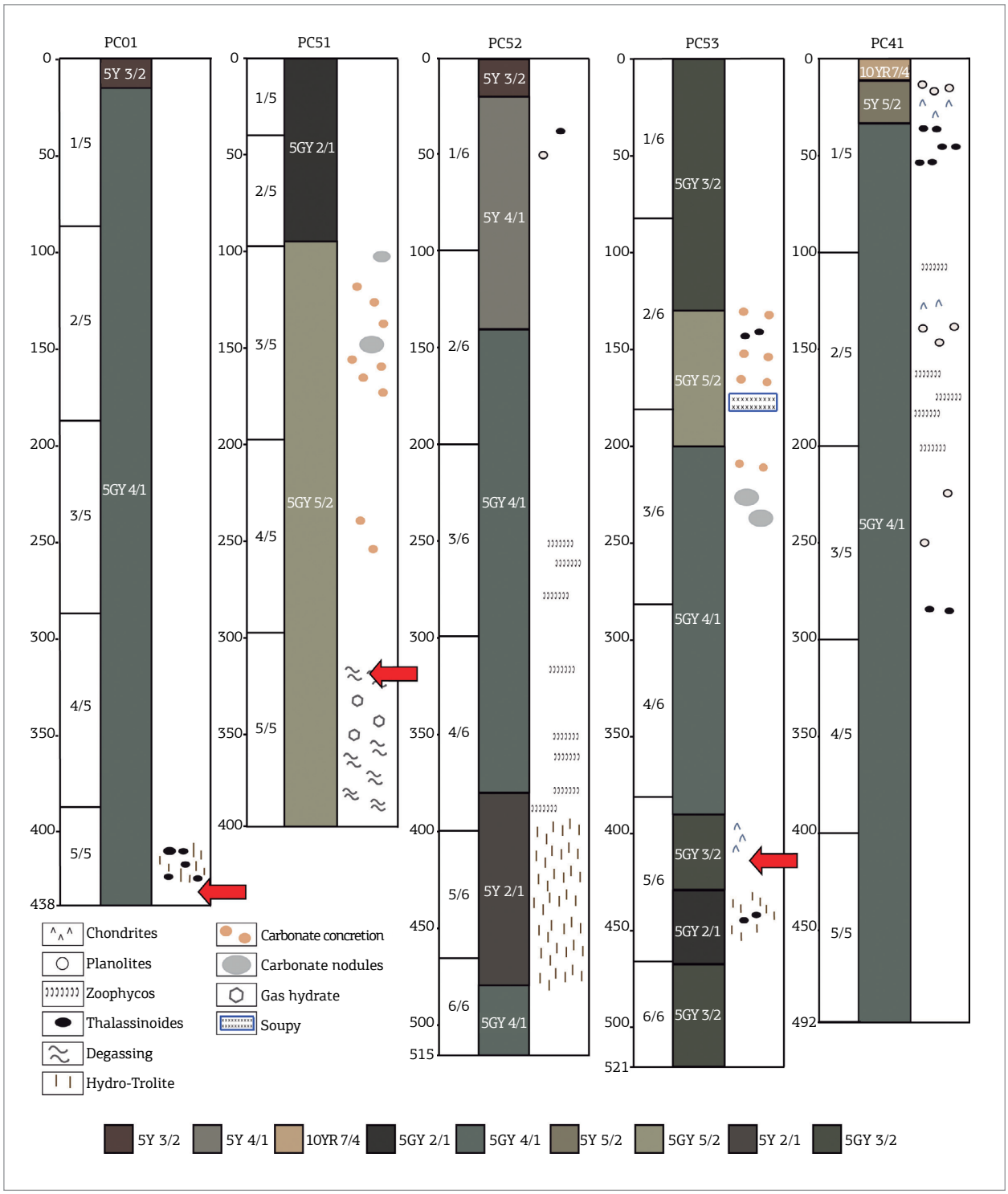

Figure 3. Main sedimentary features identified in the studied piston cores. Core units are divided based on sections cut into 100 cm. The arrows indicate the sulfate/methane interface positions in the cores. The sulfate/methane interfaces in PC41 and PC52 occur below the base of the core.

PC53 (5.21 m long/540 m water depth) contains a green gray mud with a soupy interval at 182 cmbsf. The occurrence of authigenic carbonate nodules was verified from 220 to 240 cmbsf and hydrotroilite from 435 to 470 cmbsf associated with Thalassinoides ichnofossils (460 cmbsf).

PC51 (3.97 m long/535 m water depth) consists of a dark green gray mud with concretions and carbonate nodules between 100 cm and 180 cmbsf. At the interval from 185 m to 270 cmbsf, authigenic carbonate nodules are present. Between 315 and 397 cmbsf degassing structures were described, and gas hydrates were found at interval 345–365 cmbsf. A core section showing degassing features in muddy sediments from PC51 is depicted in Fig. 4A and carbonate concretions from PC53 are shown in Fig. 4B.

The background sample in PC41 (4.92 m length/1,301 m water depth) contains a grayish orange mud in the top10 cmbsf, changing to a light olive gray (10–33 cmbsf) and olive gray below until the bottom of the core. Planolites and Chondrites (10–33 cmbsf) and Zoophycos ichnofossils with Planolites and Thalassinoides (between 100–210 cmbsf) were also described.

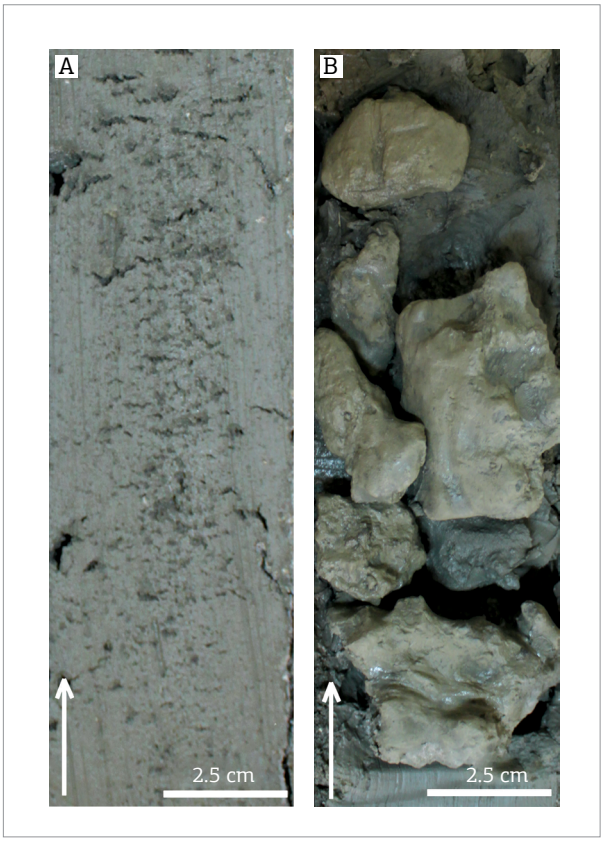

Figure 4. Detailed core pictures showing: (A) degassing features in muddy sediments (PC51 – 370 to 390 cmbsf); (B) carbonate concretions (PC53– 210 to 240 cmbsf).

Interstitial water and gas analyses

In PC41 (background), the sulfate concentration decreases slowly between 20 and 470 cmbsf from 2,800 to 1,590 ppm. The methane concentration is very low (around4 ppm) and alkalinity increases gradually from 150 to 700 ppm (Fig. 5A). The sulfate/depth profile in PC52 (Fig. 5B) shows a concave-up shape and the SR begins approximately at 60 cmbsf, with decreasing sulfate concentration from 3,227 to 692 mg L^{-1}. The methane concentration is low (200 ppm at 500 cmbsf) (Fig. 5A). Alkalinity concentration increases from 200 to 1,400 mg L^{-1} in the interval between 20 and 500 cmbsf. For PC01, the sulfate depth profile decreases linearly between 20 and 422 cmbsf, and the methane concentration increases sharply after 400 cmbsf, reaching values of 20,000 ppm (Fig. 5C). At this depth (400 cmbsf), the sulfate concentration in pore water falls to nearly zero and alkalinity increases from 200 to 1,800 mg L^{-1} (Fig. 5C). In PC51 and PC53, the SR begins approximately at 60 cmbsf, and sulfate concentration decreases from 3,110 to nearly 0.0 mg L^{-1} (Figs. 5D and 5E). In PC51, the methane concentration increases sharply from 900 to 13,000 ppm in the interval from 200 to 400 cmbsf, and alkalinity increases from 190 to 1,600 mg L^{-1} in the measured interval (Fig. 5D). In PC53, the methane concentration increases for 400 to over 20,000 ppm in the interval from 200 to 400 cmbsf, and the increase in alkalinity was from 350 to 1,700 mg L^{-1} in the measured interval (Fig. 5E). In all cores, sulfate concentrations displayed decreases from a maximum of 3,370 mg L^{-1} to values near zero in the interval between 2.6 and 500 cmbsf.

Tables 1-4 show the results for sulfate, alkalinity and methane determination in the PC52, PC01, PC51 and PC53. These results can be find in the suplementary material.

DISCUSSION

The SR process in pore waters of marine sediments involves simultaneous oxidation of methane or organic compounds and reduction of dissolved sulfate to hydrogen sulfide and bicarbonate by microorganisms (Berner 1981). Methane hydrate formation near the seafloor typically occurs below the SMI and immediately above this interface, as the SR process consumes dissolved methane and inhibits hydrate formation. The depth to which hydrate is formed is constrained by a balance between downward diffusing sulfate and the upward flux of methane towards the seafloor (Borowski *et al.* 1996).

The profile of sulfate concentrations in interstitial water in PC52 can be divided into two sections (Fig. 5). A sharp

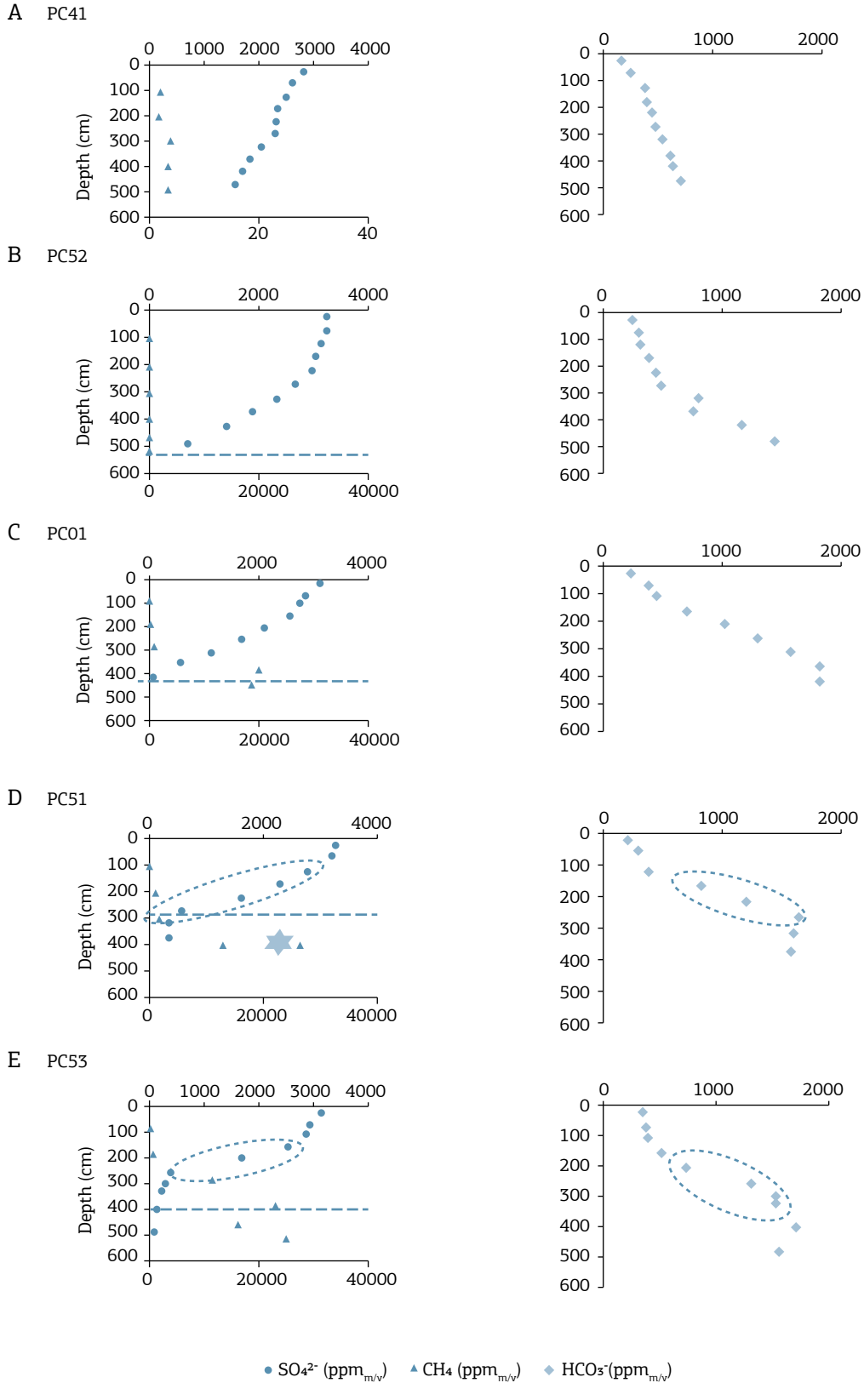

Figure 5. Sulfate and methane concentrations and alkalinity changes with depth: sulfate (circle), methane (triangle), alkalinity (lozenges), and gas hydrates occurrence (star). The dashed horizontal line indicates the positions interpreted as the sulfate/methane interface, and the dotted line is concretion-bearing interval. The letters correspond to the following PCs: (A) PC41; (B) PC52; (C) PC01; (D) PC51; (E) PC53.

Table 1.Results for sulfate, alkalinity and methane determination in PC52.

Depth (cmbsf)	SO_4^{2-} ($ppm_{m/v}$)	HCO_3^- ($ppm_{m/v}$)	CH_4 ($ppm_{v/v}$)
20	3227	250	–
70	3209	298	–
100	–	–	11.33
120	3111	305	–
170	3005	381	–
200	–	–	13.67
220	2944	438	–
270	2655	484	–
300	–	–	14.02
320	2337	785	–
370	1885	759	–
400	–	–	16.44
420	1397	1164	–
466	–	–	20.12
485	692	1436	–
515	–	–	241.87

Table 2.Results for sulfate, alkalinity and methane determination in PC01.

Depth (cmbsf)	SO_4^{2-} ($ppm_{m/v}$)	HCO_3^- ($ppm_{m/v}$)	CH_4 ($ppm_{v/v}$)
20	3121	230	–
70	2831	374	–
87	–	–	137.3
107	2735	438	–
157	2512	692	–
187	–	–	249.1
207	2092	1014	–
257	1700	1295	–
287	–	–	641.55
307	1154	1578	–
357	590	1828	–
387	–	–	19784.67
422	83	1817	–
438	–	–	18296.09

Table 3.Results for sulfate, alkalinity and methane determination in PC51.

Depth (cmbsf)	SO_4^{2-} ($ppm_{m/v}$)	HCO_3^- ($ppm_{m/v}$)	CH_4 ($ppm_{v/v}$)
20	3211	193	–
60	3143	287	–
97	–	–	127.86
117	2739	390	–
167	2252	821	–
197	–	–	904.07
217	1588	1188	–
267	528	1633	–
297	–	–	1616.88
317	310	1597	–
372	279	1573	–
497	–	–	26145.22
497	–	–	13187.69

Table 4. Results for sulfate, alkalinity and methane determination in PC53.

Depth (cmbsf)	SO_4^{2-} ($ppm_{m/v}$)	HCO_3^- ($ppm_{m/v}$)	CH_4 ($ppm_{v/v}$)
20	3117	349	–
70	2891	370	–
82	–	–	175.35
102	2856	396	–
152	2513	514	–
182	–	–	423.08
202	1651	729	–
252	344	1300	–
282	–	–	11459.02
302	242	1535	–
325	171	1522	–
382	–	–	23123.23
402	81	1687	–
467	–	–	15944.11
487	45	1529	–
521	–	–	24738.11

kink in the sulfate concentration profile at 250 cmbs is that both sediment sections have different gradients. The sulfate gradient of the upper part was probably formed in a sediment sequence with a low sulfate gradient while lower part was formed with a high gradient. This difference might be attributed to different upward flux of methane (Berner 1980). According to Borowski *et al.* (1996), rate of sulfate consumption and steepness of sulfate gradients are controlled by methane flux from below. Therefore, the low angle profile of lower part (below 250 cmbsf) is attributed to higher flux than the upper part (until 250 cmbsf). Extrapolation of the concentration profiles of dissolved CH_4 and sulfate would indicate that the SMI is positioned approximately at 550 cmbsf (Fig. 5), and hence located below the base of the core. The presence of abundant hydrotroilite at the base of the core (*i.e.*, 380–470 cmbsf) is indicative of the consumption of methane by microbial SR and release of sulfide to pore waters (Eq. 1) (Borowski *et al.* 1996, 1997). In this interval, the sulfide ions have reacted with available iron to form iron sulfide. This geochemical phenomenon explains the close association of hydrotroilite with the increase of alkalinity in the interstitial water (Fig. 5) (Niewöhner *et al.* 1998, Hinrichs *et al.* 1999).

The sulfate profile of PC01 also presents a kink-type profile at 200 cmbsf, which is indicative of variable rather than strictly high upward methane flux. A low sulfate gradient is until 200 cmbsf, and a constant linear decrease in sulfate concentration is observed below 200 cmbsf (Fig. 5), which might be attributed to high upward flux of methane coupled with high sulfate diffusion from sea water, used for anaerobic methane oxidation (Borowski *et al.* 1996, 1997). Linear sulfate profiles indicate that sulfate consumption is driven by high upward flux of methane and the slope of the concentration profile of sulfate indicates that its depletion is driven by methane flux from below. Comparison of the slope between the linear behavior regions of PC52 and PC01 shows that the slope of PC01 is lower than PC52, which means that sulfate consumption driven by methane flux from below in PC01 is higher than PC52. Based on the methane and sulfate concentration profiles, the SMI in PC01 is interpreted at422 cmbsf, which coincides with the ubiquitous presence of hydrotroilite immediately above this depth (*i.e.*, 420–430 cmbsf), associated with anaerobic oxidation reactions (Eq. 1).Although carbonate concretions are not present in the core, its alkalinity increases from 200 to 1,800 mg L^{-1} from 60 and 420 cmbsf.

The irregular pore water SO_4^{2-} profile of PC51 and PC53(Fig. 5) is credited to variations in the rates of vertical methane flux (Borowski *et al.* 1996, 1997).Two kinks can be roughly distinguished in both profiles:

- A downward kink at 117 cmbsf for PC51 and152 cmbsf for PC53;
- An upward kink at near 300 cmbsf for PC51 and PC53 to the base of piston core.

Therefore, based in sulfate profile, the variable methane flux can be divided in three stages:

- Low methane flux from 0–117 cmbsf to PC51 and from 0–152 cmbsf to PC53;
- High methane flux between 117–300 cmbsf to PC51 and 152–300 cmbsf to PC53, which corresponds to the concretion-bearing interval;
- Low methane flux from 300 cmbsf to base of piston core.

However, even showing high slope in sulfate profile in this depth, the geochemical data showed high concentration of methane (around 20,000 ppm) and gas hydrate formation (PC51).The methane profile is crossing the SMI, which suggests that the AOM does not consume all the available methane migrating through the zone of major AOM activity (Knab *et al.* 2009, Reeburgh *et al.* 1991, Jørgensen *et al.* 2001, Hensen *et al.*2003). AOM of this type, having such methane-tailing profiles, is referred as "sluggish" and it is generally associated with variable methane flux rates (Jørgensen *et al.*2001). In the same way, the sulfate profile after 300 cmbsf is continuing and showing a constant low concentration. It remains unclear why the microorganisms cannot bring down the substrate concentrations further and shorten the lifetime of coexisting methane and sulfate. Little is known about their limiting the efficiency of the anaerobic methane oxidizing microorganisms (Jørgensen *et al.* 2001). Since the gradients have not significantly smoothed, the event at PC51 and PC53 has probably occurred very recently like a magnitude of the mass (re-)movements, for example. After some hundreds of years, the kink-type sulfate profile will change to a concave up shape (Hensen *et al.* 2003).

In PC51, extrapolation of the concentration profiles of dissolved CH_4 and sulfate would indicate that the SMI is positioned approximately between 260 and 360 cmbsf. The presence of degassing features (Fig. 4) in the interval from 310 to 397 cmbsf and gas hydrate formation within this zone (345–360 cmbsf) are indicative of high methane flux (Hiruta *et al.* 2009). Pore water collected from the sediment closer to hydrate revealed the highest methane concentration (26,000 ppm) in the core, most probably derived from the dissociation of methane hydrate. The increase in alkalinity is coupled with the presence of carbonate concretions (Fig. 4B) and hydrotroilite, indicating AOM and concomitant SR. The interception depth between sulfate and methane profiles in PC53 is encountered at 300 cmbsf.

The decrease in methane concentration above the SMI is indicative of methane consumption by AOM, whereas in the region below the SMI there is methane production by methanogenesis and/or methane flux from deeper sediments via gas chimneys (Fig. 2). The increase in alkalinity is coupled with the presence of carbonate concretions (Fig. 4B) and hydrotroilite, indicating AOM and concomitant SR.

Several locations indicates a relationship and co-occurrence between venting of methane-rich fluids, gas hydrate and the formation of authigenic carbonates at the seafloor — *e.g.*, the Sea of Okhotsk (Soloviev &Ginsburg 1997), the Cascadia Margin (Bohrmann *et al.* 1998) and the Blake Ridge (Paull *et al.* 1995), Rio Grande Cone (Miller *et al.* 2015). Besides the authigenic carbonates have been shown to occur in sediments containing CH_4 hydrates, they are often associated with faults that act as conduits for the upward migration of fluids and CH_4 (Bohrmann *et al.* 1998). The favoring precipitation of authigenic carbonate minerals in the shallow subsurface by the reaction (Eq. 3) (Baker & Burns 1985):

$$2\ HCO_3^- + Ca^{2+} \leftrightarrow CaCO_3^- + CO_2 + H_2O \qquad (3)$$

In which:
HCO_3^- = hydrogencarbonate
Ca^{2+} = calcium
$CaCO_3$ = calcium carbonate
CO_2 = carbon dioxide
H_2O = water

It was identified abundant concretions and nodules in the piston cores PC51 and PC53. By correlating the stratigraphic position of the concretions bearing intervals and sulfate profiles, it is possible to do the correlations between high methane fluxes and the occurrence of concretions (Fig. 5). Therefore, high upward methane flux leads to the ascension of the SMI throughout the sedimentary column and the formation of concretions and nodules carbonates.

In addition to the use of methane and sulfate concentration profiles, the study also demonstrated that the positioning of the SMI in sediments could be inferred in high-resolution SBP sections, as the SMI is marked by a discontinuous seismic reflection (Fig. 2). The lateral changes in methane flux rates observed in different piston cores agree well with the wavy form of the SMI reflection in the profiler section, where areas of higher and lower fluxes coincide with the upward and downward displacements of the reflection, respectively. The SMI reflection is absent in areas of very low methane flux (Fig. 2). The wavy SMI-coincident reflector was sampled by cores PC51 and PC53 which contain carbonate nodules and concretions. It is thus probable that the dispersed authigenic carbonate is responsible for these reflections.

CONCLUSIONS

The methane and sulfate concentrations and alkalinity profiles in pore waters provide valuable insight into geochemical zones in methane hydrate-bearing deep sea sediments. The decrease of sulfate concentrations in the pore waters is attributed to the decomposition of organic matter and/or methane consumption by microorganisms during anaerobic oxidation of methane, which results in reduction of sulfates into sulfides. In our study area, the data imply the depth of the SMI below the seafloor is mainly controlled by the rate of the upward methane flux. The depth of the SMIs in high methane flux areas, which are associated with underlying gas chimneys, is between 3–4 m below seafloor, whereas in adjacent areas the depth of SMI is >5 m. These SMI depths in sediments can also be inferred in high-resolution SBP sections.

The shape of methane and sulfate concentration profiles in the sediments can be linked to the local methane flux rate as such:

- A near linear sulfate profiles indicate that sulfate consumption is driven by high upward flux of methane from below.
- The irregular pore water profiles, also referred as "sluggish" profiles, are correlated to variable methane flux rates.
- Concave-up exponential profiles are related to slow upward flux of methane.

The areas in which a high methane flux was identified are spatially associated with gas chimneys in sediments within pockmarks, whereas profiles with low methane flux are associated to adjacent areas.

The presence of gas chimneys in sediments can be acoustically detected using SBP images (3.5 kHz). These chimneys appear as blanking in the acoustic signals and can therefore be mapped in the subsurface. Cores identified with high methane flux are positioned above such blanking features and low methane flux in cores adjacent to them. Also, higher amplitude reflections following the SMI seem to occur where authigenic carbonate nodules and concretions are present.

ACKNOWLEDGEMENTS

The authors thank PETROBRAS for sponsoring this research and for the permission to publish this paper, the IHS Global Inc. Educational/Academic Grant Program for the use of the Kingdom Software, and the Brazilian National Council for Scientific and Technological Development (CNPq) for financial support.

REFERENCES

Baker P.A., Burns S.J. 1985. Occurrence and formation of dolomite in organic-rich continental margin sediments. *American Association Of Petroleum Geologists Bulletin*, **69**(11):1917-1930.

Berner R.A. 1980. *Early Diagenesis: A Theoretical Approach*. Princeton University Press, Princeton, 241 p.

Berner R.A. 1981. A new geochemical classification of sedimentary environments. *Journal of Sedimentary Research*,**51**(2):359-365.

Bohrmann G., Greinert J., Suess E., Torres M.1998. Authigenic carbonates from Cascadia subduction zone and their relation to gas hydrate stability. *Geology*, **26**(7):647-650.

Borowski W.S., Paull C.K., Ussler W. 1996. Marine pore-water sulfate profiles indicate in situ methane flux from underlying gas hydrate. *Geology*, **24**(7):655-658.

Borowski W.S., Paull C.K., Ussler W. 1997. Carbon cycling within the upper methanogenic zone of continental rise sediments; An example from the methane-rich sediments overlying the Blake Ridge gas hydrate deposits. *Marine Chemistry*, **57**(3-4):299-311.

Borowski W.S., Paull C.K., Ussler W. 1999. Global and local variations of interstitial sulfate gradients in deep-water, continental margin sediments: Sensitivity to underlying methane and gas hydrates. *Marine Geology*, **159**(1-4):131-154.

Breland J.A., Byrne R.H. 1993. Spectrophotometric procedures for determination of sea water alkalinity using bromocresol green. *Deep Sea Research Part I: Oceanographic Research Papers*, **40**(3):629-641.

Carroll J.J. 1992. Comments on 'The prediction of methane solubility in natural waters to high ionic strength from 0 to 2508C and from 0 to 1600 bar'. *In*: Duan Z., Moller N., Greenberg J., Weare J.H. (eds.) *Geochemica Cosmochemica Acta*, 56, p. 4301-4302.

Claypool G.E., Kaplan I.R. 1974. The origin and distribution of methane in sediments. *In*: Kaplan I.R. (ed.) *Natural Gases in Marine Sediments*. New York, Plenum, p. 99-139.

Clennell M.B.2000. Hidrato de gás submarino: natureza, ocorrência e perspectivas para exploração na margem continental brasileira. *Revista Brasileira de Geofísica*, **18**(3):397-409.

Demirbas A. 2010. Methane hydrates as potential energy resource: Part 1 – Importance, resource and recovery facilities. *Energy Conversion and Management*, **51**(7):1547-1561.

Fontana R.L., Mussumeci A. 1994. Hydrates offshore Brazil. *Annals of the New York Academy of Sciences*, **715**:106-113.

Freire A.F.M., Matsumoto R., Santos L.A. 2011. Structural-stratigraphic control on the Umitaka Spur gas hydrates of Joetsu Basin in the eastern margin of Japan Sea. *Marine and Petroleum Geology*, **28**(10):1967-1978.

Gupta A.K. 2004. Marine gas hydrates: their economic and environmental importance. *Current Science*, **86**(9):1198-1199.

Hinrichs K., Hayes J.M., Sylva S.P., Brewer P.G., DeLong E.F. 1999. Methane-consuming archaebacteria in marine sediments. *Nature*, **398**:802-805.

Hiruta A., Snyder G.T., Tomaru H., Matsumoto R.2009. Geochemical constraints for the formation and dissociation of gas hydrate in an area of high methane flux, eastern margin of the Japan Sea. *Earth and Planetary Science Letters*, **279**(3-4):326-339.

Hensen C., Zabel M., Pfiefer K., Schwenk T., Kasten S., Riedinger N., Schulz H.D., Boetius A. 2003. Control of sulfate pore-water profiles by sedimentary events and the significance of anaerobic oxidation of methane for the burial of sulfur in marine sediments. *Geochimica et Cosmochimica Acta*, **67**(14):2631-2647.

Jørgensen B.B., Weber A., Zopfi J. 2001. Sulfate reduction and anaerobic methane oxidation in Black Sea sediments. *Deep Sea Research Part I: Oceanographic Research Papers*, **48**(9):2097-2120.

Joye S.B., Boetius A., Orcutt B.N., Montoya J.P., Schulz H.N., Erickson M.J., Lugo S.K. 2004. The anaerobic oxidation of methane and sulfate reduction in sediments from Gulf of Mexico cold seeps. *Chemical Geology*, **205**(3-4):219-238.

Kennicutt M.C., Brooks J.M., Bidigare R.R., Denoux G.J. 1988b. Gulf of Mexico hydrocarbon seep communities — I. Regional distribution of hydrocarbon seepage and associated fauna. *Deep Sea Research Part A. Oceanographic Research Papers*, **35**(9):1639-1651.

Kennicutt M.C., Brooks J.M., Denoux G.J. 1988a. Leakage of deep, reservoired petroleum to the near surface on the gulf of Mexico Continental slope. *Marine Chemistry*, **24**(1):39-59.

Knab N.J., Cragg B.A., Hornibrook E.R.C., Holmkvist L., Pancost R.D., Borowski C., Parkes R.J., Jørgensen B.B. 2009. Regulation of anaerobic methane oxidation in sediments of the Black Sea. *Biogeosciences*, **6**:1505-1518.

Martins L.R., Melo U., França A.M.C., Santana C.I.,Martins I.R. 1972. Distribuição Faciológica da Margem Continental Sul Riograndense. Congresso Brasileiro de Geologia. 26° Anais. Belém, Brasil, p. 115-132.

Matsumoto R., Ryu B., Lee S., Lin S., Wu S., Sain K., Pecher I., Riedel M.2011. Occurrence and exploration of gas hydrate in the marginal seas and continental margin of the Asia and Oceania region. *Marine and Petroleum Geology*, **28**(10):1751-1767.

Michaelis W., Seifert R., Nauhaus K., Treude T., Thiel V., Blumenberg M., Knittel K., Gieseke A., Peterknecht K., Pape T., Boetius A., Amann R., Jørgenson B.B.,Widdel F., Peckmann J., Pimenov N., Gulin M.B. 2002. Microbial reefs in the black sea fueled by anaerobic oxidation of methane. *Science*, **297**(5583):1013-1015.

Miller D.J., Ketzer J.M., Viana A.R., Kowsmann R.O., Freire A.F.M., Oreiro S.G., Augustin A.H., Lourega R.V., Rodrigues L.F., Heemann R., Preissler A.G., Machado C.X., Sbrissa G.F. 2015. Natural gas hydrates in the Rio Grande Cone (Brazil): A new province in the western South Atlantic. *Marine and Petroleum Geology*, **67**:187-196.

Niewöhner C., Hensen C., Kasten S., Zabel M., Schulz H.D. 1998. Deep sulfate reduction completely mediated by anaerobic methane oxidation in sediments of the upwelling area off Namibia. *Geochimica et Cosmochimica Acta*, **62**(3):455-464.

Oliveira S., Vilhena O., da Costa E. 2010. Time-frequency spectral signature of Pelotas Basin deep water gas hydrates system. *Marine Geophysical Researches*, **31**(1-2):89–97.

Paull C.K., Ussler W., Borowski W.S., Spiess F.N. 1995. Methane-rich plumes on the Carolina continental rise: Associations with gas hydrates. *Geology*, **23**(1):89-92.

Raiswell R. 1988. Chemical model for the origin of minor limestone-shale cycles by anaerobic methane oxidation. *Geology*, **16**(7):641-644.

Reeburgh W.S., Ward B.B., Whalen S.C., Sandbeck K.A., Kilpatrick K.A., Kerkhof L.J. 1991. Black Sea methane geochemistry. *Deep Sea Research Part A. Oceanographic Research Papers*, **38**(S2):S1189-S1210.

Riedel M., Novosel I., Spence G.D., Hyndman R.D., Chapman R.N., SolemR.C., Lewis T. 2006. Geophysical and geochemical signatures associated with gas hydrate- related venting in the northern Cascadia margin. *Geological Society of America Bulletin*, **118**(1-2):23-38.

Römer M., Sahling H., Pape T., Bahr A., Feseker T., Wintersteller P., Bohrmann G. 2012. Geological control and magnitude of methane

ebullition from a high-flux seep area in the Black Sea—the Kerch seep area. *Marine Geology*, **319-322**:57-74.

Sad A.R.E., Silveira D.P., Machado D.A.P., Silva S.R.P., Maciel R.R.1998. Marine gas hydrates evidence along the Brazilian coast. *In*: Proc. AAPG International conference and exhibition. Rio de Janeiro, Brazil, CD-ROM.

Sassen R., MacDonald I.R., Guinasso Jr. N.L., Joye S., Requejo A.G., Sweet S.T., Alcalá-Herrera J., DeFreitas D.A., Schink D.R. 1998. Bacterial methane oxidation in sea-floor gas hydrate: Significance to life in extreme environments. *Geology*, **26**(9):851-854.

Silveira D.P., Machado M.A.P. 2004. Bacias sedimentares brasileiras: Bacia de Pelotas. *Boletim informativo da Fundação Paleontológica Phoenix*, **63**(6).

Soloviev V.A., Ginsburg G.D. 1997. Water segregation in the course of gas hydrate formation and accumulation in submarine gas-seepage fields. *Marine Geology*, **137**(1-2):59-68.

Tomasini J., Santa Ana H., Conti B., FerroS., Gristo P., Marmisolle J., Morales E., Rodriguez P., Soto M., Veroslavsky G. 2011.Assessment of marine gas hydrates and associated free gas distribution offshore Uruguay. *Journal of Geological Research*, **2011**(2011):1-7.

Zatsepina O.Y., Buffett B.A. 1997. Phase equilibrium of gas hydrate: Implications for the formation of hydrate in the deep sea floor. *Geophysical Research Letters*, **24**(13):1567-1570.

Available at www.sbgeo.org.br